Pergamon

Int. J. Heat Mass Transfer. Vol. 38, No. 5, pp. 935–946, 1995

0017–9310/95 $9.50 + 0.00

0017–9310(94)00198–7

Double-diffusion from a vertical surface in a porous region saturated with a non-Newtonian fluid

S. K. RASTOGI and D. POULIKAKOS†

Mechanical Engineering Department, University of Illinois at Chicago, P.O. Box 4348, Chicago, IL 60680, U.S.A.

(*Received* 4 *March* 1994 *and in final form* 16 *June* 1994)

Abstract—In this paper, a theoretical study is presented for the problem of double-diffusion from a vertical plate embedded in a porous matrix that is saturated with a non-Newtonian (power law) fluid. The study consists of two parts: In the first part, scaling analysis is utilized to obtain estimates of the quantities of interest and to identify the various possible flow regimes depending on the values of the buoyancy ratio and the Lewis number. This task is performed for both the case of a wall with constant temperature and concentration and the case of a wall with constant heat and species flux. In the second part of the study, a numerical solution of the problem is presented for the general case of a wall with arbitrarily varying temperature and concentration. The values of the relevant parameters resulting in a constant heat and species flux or a constant temperature and concentration at the wall are identified. The dependence of the flow, temperature, and concentration fields as well as of the local heat and species fluxes at the wall on the power law exponent, the buoyancy ratio and the Lewis number is documented for the two cases: (a) constant temperature and concentration, (b) constant heat and species flux.

1. INTRODUCTION

Double-diffusive convection in fluid saturated media occurs in many engineering applications exemplified by oil recovery, geothermal energy extraction, food processing, materials processing, the dispersion of chemical contaminants in various processes in the chemical industry and in the environment, and the migration of moisture in insulation and grain storage spaces. It is because of this reason that several studies have been reported in the literature that are relevant to double-diffusive convection in fluid saturated porous media. To exemplify, Poulikakos [1] studied theoretically the problem of double-diffusion from a point source situated in a porous medium. Interesting flow structures were found to exist especially in the case where the mass transfer driven flow was opposing the heat transfer driven flow. The study of Poulikakos [1] was subsequently extended to the investigation of double-diffusion from a line source in a porous medium [2].

Bejan and Khair [3] solved the problem of double-diffusion from a vertical plate embedded in a porous medium. Through scale analysis, they showed that the natural convection flow conforms to one of four possible regimes depending on the value of the concentration to thermal buoyancy ratio and the Lewis number. The scale analysis was validated by a numerical solution of the problem. Jang and Chang [4, 5] reported the effect of the wall inclination on the combined heat and mass transport phenomenon by generalizing the similarity solution approach adopted by Bejan and Khair [3]. The transient development of velocity, temperature, and concentration boundary layers near a vertical surface embedded in a porous medium was documented by Jang and Ni [6].

A number of studies have been reported in the literature focusing on the problem of double-diffusion in a porous layer heated from below. To this end, Nield [7], Taunton and Lightfoot [8] and Selimos and Poulikakos [9] have reported linear stability analyses of this problem. Rudraiah *et al.* [10] have performed a nonlinear stability analysis. Double-diffusive convection in a stably stratified porous layer destabilized by lateral heating has been studied by Gershuni *et al.* [11] and Khan and Zebib [12].

Based on the above discussion it can be concluded that the problem of double-diffusion in a fluid saturated porous medium has received some (rather recent) attention. In all the published studies discussed earlier, the fluid saturating the porous medium was assumed to be Newtonian. However, in several of the engineering applications listed at the beginning of this section (such as oil recovery, food processing, the spreading of contaminants in the environment and in various processes in the chemical and materials industry) the fluid saturating the porous matrix is not necessarily Newtonian. In our literature survey we were not able to identify any published studies on double-diffusion in a porous layer saturated with a non-Newtonian fluids. Even in the limit of thermal convection in a porous medium saturated with a non-

†Author to whom correspondence should be addressed.

NOMENCLATURE

A	constant in flow model, equations (6) and (7)
c_p	specific heat
C	concentration
D	mass diffusivity
E	energy
f	similarity streamfunction profile
F	dummy variable
g	gravitational acceleration
G	buoyancy ratio for constant temperature and concentration condition, equation (47)
G^*	buoyancy ratio for constant heat and species flux, equation (69)
H	height of the wall, Fig. 1
k	thermal conductivity
Le	Lewis number, α/D
m	permeability
n	power law index
p	pressure
P	constant in power law variation, equation (18)
q', q''	heat transfer rate per unit length and area, respectively
Q	constant in power law variation, equation (19)
Ra	thermal Rayleigh number for constant temperature and concentration, equation (26)
Ra^*	thermal Rayleigh number for constant heat and species flux, equation (59)
S	similarity concentration profile
Sh	Sherwood number
T	temperature
u	velocity in the x-direction, Fig. 1
v	velocity in the y-direction, Fig. 1
$\mathbf{v}$	velocity vector
x, y	Cartesian coordinates, Fig. 1
w', w''	rate of mass transfer per unit length and area, respectively.

Greek symbols

α	thermal diffusivity
β	coefficient of thermal expansion
β_C	coefficient of concentration expansion
δ_C	concentration boundary layer thickness
δ_T	thermal boundary layer thickness
Γ	consistency index
η	similarity variable
θ	similarity temperature profile
λ	exponent in power law variation, equations (18) and (19)
μ	viscosity
ρ	density
Ψ	streamfunction.

Subscripts

a	apparent
o	wall property
y	local quantity
∞	far field.

Newtonian fluid driven by temperature gradients alone, the number of existing works is very limited. To this end, Chen and Chen [13] studied numerically the problem of boundary layer free convection (driven by temperature gradients) about an isothermal vertical plate in a porous medium saturated by a power law fluid. They found a significant dependence of the temperature field and the heat transfer rate from the plate on the power law index. Poulikakos and Spatz [14] investigated the effect of non-Newtonian natural convection at a melting front in a permeable matrix. Their results documented the dependence of the local heat transfer rate at the melting front as well as the dependence of the temperature and flow fields in the melt, on the type of power law fluid saturating the porous matrix.

The present study investigates the basic problem of boundary layer double-diffusion from a vertical plate embedded in a porous material saturated with a power law fluid. Scaling analysis is performed to identify the various flow, heat transfer and mass transfer regimes for both cases when the plate is isothermal and of constant concentration as well as when the heat and species fluxes at the plate are constant. A numerical solution of the problem is also presented such that the plate temperature and concentration are allowed to vary arbitrarily with distance along the plate. The constant plate temperature and concentration case as well as the case of constant heat and mass fluxes at the plate are extracted as specific results of the general formulation.

2. MATHEMATICAL FORMULATION

Consider the boundary layer flow in the vicinity of an impermeable vertical plate embedded in a porous medium which is saturated by a power law fluid, as shown in Fig. 1. The temperature and the concentration (of a certain constituent) of the porous medium far away from the plate are denoted by T_∞, C_∞. A host of possibilities for the boundary conditions at the plate will be considered later in this section. Because of this fact, temperature and concentration gradients exist in the system which yield a buoyancy-driven flow. The present study focuses on the case where this flow is of the boundary layer kind as exemplified by the schematic of Fig. 1.

The boundary layer equations governing the con-

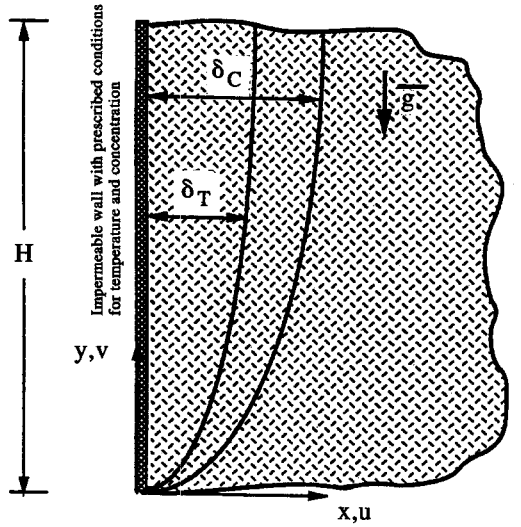

Fig. 1. Schematic of the double-diffusive boundary layer of interest and the coordinate system.

servation of mass, momentum, energy and species are [15–18]

$$\frac{\partial u}{\partial x}+\frac{\partial v}{\partial y}=0 \tag{1}$$

$$u=-\frac{m}{\mu_a}\frac{\partial p}{\partial x} \tag{2}$$

$$v=-\frac{m}{\mu_a}\left(\frac{\partial p}{\partial y}+\rho g\right) \tag{3}$$

$$u\frac{\partial T}{\partial x}+v\frac{\partial T}{\partial y}=\alpha\frac{\partial^2 T}{\partial x^2} \tag{4}$$

$$u\frac{\partial C}{\partial x}+v\frac{\partial C}{\partial y}=D\frac{\partial^2 C}{\partial x^2}. \tag{5}$$

In the above equations, x and y are the Cartesian coordinates (Fig. 1), u and v the Cartesian velocity components (Fig. 1), p the pressure, T the temperature, C the species concentration, ρ the density, α the effective thermal diffusivity, D the effective species diffusivity and m the permeability of the porous medium. The apparent viscosity, μ_a, of the porous matrix saturated with a power law fluid with zero yield stress is given by [15, 16]

$$\mu_a = A|\bar{\nabla}|^{n-1}$$
$$= A(u^2+v^2)^{(n-1)/2}. \tag{6}$$

The constant A in the equation (6) is related to the rheological parameters (the power law index n and the consistency index Γ) and the properties (the permeability m and the porosity ϕ of the porous medium) as follows:

$$A=\frac{2\Gamma}{(8)^{(n+1)/2}(m\phi)^{(n-1)/2}\left(\frac{n}{1+3n}\right)^n}. \tag{7}$$

Note that for a Newtonian fluid ($n=1$), equations (6) and (7) yield $A=\Gamma=\mu_a$, where μ_a is now the Newtonian effective viscosity and Darcy's law is recovered. Introducing the Boussinesq approximation in the buoyancy term of the momentum equation (3)

$$\rho=\rho_\infty[1-\beta(T-T_\infty)-\beta_C(C-C_\infty)] \tag{8}$$

where β and β_C are the coefficients of thermal and concentration expansion, and eliminating the pressure between equations (2) and (3), yields (in the boundary layer limit)

$$\frac{\partial v^n}{\partial x}=\frac{mg\rho_\infty}{A}\left(\beta\frac{\partial T}{\partial x}+\beta_C\frac{\partial C}{\partial x}\right). \tag{9}$$

To complete the mathematical formulation of the problem, the boundary conditions need to be discussed. The velocity boundary conditions are the non-permeability of the vertical plate and the motionless state of the fluid far away from the plate:

$$x=0:\quad u=0 \tag{10}$$

$$x\to\infty:\quad v=0. \tag{11}$$

As mentioned earlier, far from the plate the temperature and concentration are constant:

$$x\to\infty:\quad T=T_\infty\quad C=C_\infty. \tag{12, 13}$$

Regarding the wall thermal and concentration conditions three cases will be examined: initially, scaling analysis will be performed for two situations. First the case where the plate is at constant temperature and concentration:

$$x=0:\quad T=T_0=\text{constant}\quad C=C_0=\text{constant} \tag{14, 15}$$

and, second, the case where the heat and species fluxes at the plate are constant:

$$x=0:\quad -k\frac{\partial T}{\partial x}=q''\quad -D\frac{\partial C}{\partial x}=w''. \tag{16, 17}$$

In the above equations, the subscript "0" denotes the wall, k is the effective thermal conductivity of the porous medium, q'' is the wall heat flux and w'' the wall species flux. The remaining quantities have been defined earlier.

Subsequently, the problem will be solved numerically for the general case where the wall temperature and concentration vary arbitrarily:

$$x=0:\quad T=T_0=T_\infty+Py^\lambda\quad C=C_0=C_\infty+Qy^\lambda \tag{18, 19}$$

where P, Q and λ are constants. With no loss of generality it is assumed that both P and Q are positive constants ($P>0$, $Q>0$). Before closing this section, we note that equation (9) can be integrated explicitly

in the x-direction between an arbitrary point inside both the boundary layers and a point at "infinity" (outside both the boundary layers). This integration reduces the order of equation (9) and facilitates the solution process. The result reads [after applying boundary conditions, equations (10)–(13)]

$$v^n = \frac{mg\rho_\infty}{A}[\beta(T-T_\infty)+\beta_C(C-C_\infty)]. \quad (20)$$

3. SCALING ANALYSIS

3.1. *Constant wall temperature and species concentration*

In this case, the mathematical model consists of equations (1), (4), (5), (10)–(15) and (20). At the onset of the scaling analysis appropriate scales of the various quantities are selected whenever possible. An extensive discussion on scaling analysis and its application in convective heat transfer is included in ref. [19]. The notation used in this section is the same to the notation of the previous section with the understanding that the symbols denote the scales of the actual quantities.

To facilitate the scaling analysis, beginning with the definition of a vertical velocity scale, two limits will be examined sequentially: heat transfer driven flow and mass transfer driven flow.

3.1.1. *Heat transfer driven flow.* In this case, the thermal gradients dominate over the concentration gradients in the buoyancy force, i.e.

$$|\beta(T_0-T_\infty)| \gg |\beta_C(C_0-C_\infty)|. \quad (21)$$

The scale for the vertical velocity is obtained directly from equation (20):

$$v \sim \left[\frac{mg\rho_\infty\beta(T-T_\infty)}{A}\right]^{1/n}. \quad (22)$$

Applying scaling to the energy equation (4) inside the thermal boundary layer (of extent $\delta_T xH$) yields

$$u\frac{T_0-T_\infty}{\delta_T}+v\frac{T_0-T_\infty}{H} \sim \alpha\frac{T_0-T_\infty}{\delta_T^2}. \quad (23)$$

At the same time from the continuity equation

$$\frac{u}{\delta_T} \sim \frac{v}{H}. \quad (24)$$

Combining equations (22)–(24), we conclude that, in order of magnitude sense,

$$\delta_T \sim H(Ra)^{-1/2n} \quad (25)$$

where the Darcy-modified Rayleigh number is defined as

$$Ra = \frac{mg\rho_\infty\beta(T_0-T_\infty)H^n}{A\alpha^n}. \quad (26)$$

The overall Nusselt number scale is obtained directly from the definition of the Nusselt number

$$Nu = \frac{q'}{k(T_0-T_\infty)}. \quad (27)$$

Taking into account that

$$q' \sim kH\frac{T_0-T_\infty}{\delta_T} \quad (28)$$

and invoking equation (25) yields

$$Nu \sim (Ra)^{1/2n}. \quad (29)$$

Despite the fact that the flow is driven by temperature gradients in the present limit, mass transfer occurs since the constituent in the mixture is carried along with the flow and species diffusion occurs simultaneously. The overall mass transfer from the wall is described by the Sherwood number

$$Sh = \frac{w'}{D(C_0-C_\infty)}. \quad (30)$$

Recognizing that the mass transfer rate per unit length scales as

$$w' \sim DH\frac{C_0-C_\infty}{\delta_C} \quad (31)$$

the Sherwood number scale is expressed as

$$Sh \sim \frac{H}{\delta_C}. \quad (32)$$

To obtain the scale of δ_C is not straightforward. As discussed in detail in Bejan and Khair [3] this scale depends on the relative magnitude of δ_T and δ_C. Since this discussion can be easily found in ref. [3], it will not be repeated here for brevity.

To proceed, we integrate the species conservation equation (5) across the double boundary layer starting from the wall to a point (x) outside both δ_T and δ_C:

$$\frac{d}{dy}\int_0^{x>\max(\delta_T,\delta_C)} v(C-C_\infty)\,dx = -D\left(\frac{\partial C}{\partial x}\right)_{x=0}. \quad (33)$$

In terms of scaling, equation (33) becomes

$$\frac{v(C_0-C_\infty)}{H}\min(\delta_T,\delta_C) \sim D\frac{(C_0-C_\infty)}{\delta_C}. \quad (34)$$

As explained in detail by Bejan and Khair [3], the utilization of the term min (δ_T, δ_C) in equation (34) is necessary to assure that we are dealing with a layer that moves upward because of thermal gradients and, at the same time, is rich in the species diluted in the mixture.

(a) $\delta_C \ll \delta_T$

In this case, min $(\delta_T, \delta_C) = \delta_C$ and equation (34) together with equation (22) yields

$$\delta_C \sim HLe^{-1/2}Ra^{-1/2n} \quad (35)$$

where the Lewis number is defined as usual:

$$Le = \alpha/D. \quad (36)$$

Combining equations (32, 35) we obtain

$$Sh \sim Le^{1/2}\, Ra^{1/2n}. \tag{37}$$

Comparing the scales of the thermal to the concentration boundary layers, we discover that [equations (25) and (35)]

$$\frac{\delta_C}{\delta_T} \sim Le^{-1/2}. \tag{38}$$

Hence, the condition $\delta_C \ll \delta_T$ is equivalent to $Le \gg 1$.

(b) $\delta_C \gg \delta_T$

In this case, equation (34) yields, after taking into account equations (22) and (25),

$$\delta_C \sim H\, Le^{-1}\, Ra^{-1/2n}. \tag{39}$$

Utilizing equation (39) and the scale for Sh, equation (34),

$$Sh \sim Le\, Ra^{1/2n}. \tag{40}$$

Again, comparing the scales for δ_C and δ_T, equations (25) and (39), we see that

$$\frac{\delta_C}{\delta_T} \sim Le^{-1}. \tag{41}$$

Hence, the limit $\delta_C \gg \delta_T$ is equivalent to $Le \ll 1$.

3.1.2. *Mass transfer driven flows.* For the flow to be driven by concentration gradients alone

$$|\beta(T_0 - T_\infty)| \ll |\beta_C(C_0 - C_\infty)|. \tag{42}$$

The momentum equation (20) in this case yields the following vertical velocity scale:

$$v \sim \left[\frac{mg\rho_\infty \beta_C (C_0 - C_\infty)}{A}\right]^{1/n}. \tag{43}$$

The scaling equivalent of the species concentration equation (5) in the region ($\delta_C x H$) is

$$u\frac{C_0 - C_\infty}{\delta_C} + v\frac{C_0 - C_\infty}{H} \sim D\frac{C_0 - C_\infty}{\delta_C^2}. \tag{44}$$

The scaling equivalent of the continuity equation in the same region is

$$\frac{u}{\delta_C} \sim \frac{v}{H}. \tag{45}$$

Combining equations (43)–(45), we obtain the following scale for the concentration boundary layer thickness:

$$\delta_C \sim H\, Le^{-1/2}\, Ra^{-1/2n} |G|^{-1/2n} \tag{46}$$

where the buoyancy ratio is defined as

$$G = \frac{\beta_C (C_0 - C_\infty)}{\beta (T_0 - T_\infty)}. \tag{47}$$

The parameter G measures the relative importance of mass and thermal diffusion in the buoyancy driven flow. Clearly, G is zero for thermal driven flows, infinite for concentration driven flows, positive for aiding flows, and negative for opposing flows. Note that in the present limit according to equation (42), $|G| \gg 1$.

The expression for the overall Sherwood number is obtained from equations (32) and (46):

$$Sh \sim Le^{1/2}\, Ra^{1/2n} |G|^{1/2n}. \tag{48}$$

To calculate the overall Nusselt number scale, knowledge of the scale for the thermal boundary layer thickness is necessary. The procedure for obtaining the scale for δ_T is similar to the procedure followed to obtain the scale for δ_C in Section 3.1.1 (heat transfer driven flow). To this end, integrating the energy equation (4) in the x-direction from the wall to a point outside the double boundary layer structure yields

$$\frac{\mathrm{d}}{\mathrm{d}y}\int_0^{x > \max(\delta_T, \delta_C)} v(T - T_\infty)\,\mathrm{d}x = -\alpha\left(\frac{\partial T}{\partial x}\right)_{x=0}. \tag{49}$$

Scaling the above equation

$$\frac{v(T_0 - T_\infty)}{H}\min(\delta_T, \delta_C) \sim \frac{\alpha(T_0 - T_\infty)}{\delta_T}. \tag{50}$$

The appearance of the quantity min (δ_T, δ_C) was explained earlier following equation (34). Two cases need to be considered as in Section 3.1.1.

(a) $\delta_T \ll \delta_C$

In this case, equations (43) and (50) result in

$$\delta_T \sim H\, Ra^{-1/2n} |G|^{-1/2n}. \tag{51}$$

The corresponding expression for Nu is

$$Nu \sim Ra^{1/2n} |G|^{1/2n}. \tag{52}$$

Much like before, by comparing the scales for $\delta_T \ll \delta_C$ we conclude that this statement is equivalent to $Le \ll 1$.

(b) $\delta_T \gg \delta_C$

Taking into account the fact that min (δ_T, δ_C) = δ_C and combining equations (43), (46) and (50) results in

$$\delta_T \sim H\, Le^{1/2}\, Ra^{-1/2n} |G|^{-1/2n} \tag{53}$$

the expression for Nu is obtained as usual via equations (27), (28) and (53):

$$Nu \sim Le^{-1/2}\, Ra^{1/2n} |G|^{1/2n}. \tag{54}$$

In a manner analogous to what was explained earlier, it can be easily shown that $\delta_T \gg \delta_C$ is equivalent to $Le \gg 1$.

The key results of this section, both for the heat transfer driven flow and the mass transfer driven flow scenarios, are summarized in Table 1. It is worth mentioning here that in the limit of a Newtonian fluid ($n = 1$) all the results of Table 1 reduce identically to the analogous quantities of ref. [3].

3.2. *Constant wall heat and species flux*

The mathematical model remains unchanged except for the fact that the boundary conditions, equations (16), (17), replace the boundary conditions, (14) and (15), utilized in Section 3.1. Again, we will consider

Table 1. Scales of various quantities of interest for a surface at constant temperature and concentration

Driving potential		δ_T	δ_C	Nu	Sh
Temperature gradients, $\|G\| \ll 1$	$Le \gg 1$	$H(Ra)^{-1/2n}$	$HLe^{-1/2}\,Ra^{-1/2n}$	$(Ra)^{1/2n}$	$Le^{1/2}\,Ra^{1/2n}$
Temperature gradients, $\|G\| \ll 1$	$Le \ll 1$	$H(Ra)^{-1/2n}$	$HLe^{-1}\,Ra^{-1/2n}$	$(Ra)^{1/2n}$	$Le\,Ra^{1/2n}$
Concentration gradients, $\|G\| \gg 1$	$Le \ll 1$	$H(Ra\|G\|)^{-1/2n}$	$HLe^{-1/2}(Ra\|G\|)^{-1/2n}$	$(Ra\|G\|)^{1/2n}$	$Le^{1/2}(Ra\|G\|)^{1/2n}$
Concentration gradients, $\|G\| \gg 1$	$Le \gg 1$	$HLe^{1/2}(Ra\|G\|)^{-1/2n}$	$HLe^{-1/2}(Ra\|G\|)^{-1/2n}$	$Le^{-1/2}(Ra\|G\|)^{1/2n}$	$Le^{1/2}(Ra\|G\|)^{1/2n}$

sequentially the cases of heat transfer driven flow and mass transfer driven flow.

3.2.1. *Heat transfer driven flow.* Since the wall temperature and concentration are unknown and variable, we need to define at the outset, approximate scales for the characteristic temperature and concentration differences in the system (ΔT and ΔC, respectively). Utilizing the scaling equivalent of the constant flux boundary conditions, (16) and (17), yields

$$\Delta T \sim \frac{q''\delta_T}{k} \quad \Delta C \sim \frac{w''\delta_C}{D}. \tag{55, 56}$$

Note that the above scales depend on the thickness of the thermal and concentration boundary layers. For heat transfer driven flows, $|G| \ll 1$, the vertical velocity scale results directly from the momentum equation (20) accounting also for equation (55):

$$v \sim \left(\frac{mg\beta\rho_\infty \dfrac{q''\delta_T}{k}}{A}\right)^{1/n}. \tag{57}$$

The thermal boundary layer thickness is obtained from the scaling of the energy equation (4) in the region ($\delta_T x H$). The procedure is identical to what led to equation (25) with the difference that the temperature difference scale is not $(T_o - T_\infty)$ but ΔT as defined by equation (55). The final result for the thermal boundary layer thickness is

$$\delta_T \sim H(Ra^*)^{-1/(2n+1)} \tag{58}$$

where the Darcy-modified Rayleigh number for the constant heat flux case reads

$$Ra^* = \frac{mg\beta\rho_\infty H^{n+1} q''}{A\alpha^n k}. \tag{59}$$

The Nusselt number is defined as

$$Nu = \frac{\dfrac{q''}{\Delta T}H}{k} \sim \frac{H}{\delta_T}. \tag{60}$$

Combining equations (58) and (60)

$$Nu \sim (Ra^*)^{1/(2n+1)}. \tag{61}$$

As in Section 3.1, the mass transfer scales in the present case of heat transfer driven flow will be evaluated, next. The overall Sherwood number is defined as

$$Sh = \frac{\dfrac{w''}{\Delta C}H}{D} \sim \frac{H}{\delta_C}. \tag{62}$$

To obtain the scale for Sh, the scale for δ_C is needed. Following the procedure utilized in Section 3.1, the species concentration equation needs to be integrated between the wall and a point outside both the boundary layers. The outcome of this procedure yields a scaling statement identical to equation (34) with $(C_o - C_\infty)$ replaced by ΔC; equation (56). To determine the quantity min (δ_T, δ_C), as before, two cases will be considered.

(a) $\delta_C \ll \delta_T$

In this case, $\delta_C = \min(\delta_C, \delta_T)$. Equation (34) (with the above-mentioned modification) yields

$$\delta_C \sim HLe^{-1/2}(Ra^*)^{-1/(2n+1)}. \tag{63}$$

By combining equations (62) and (63), we obtain

$$Sh \sim Le^{1/2}(Ra^*)^{1/(2n+1)}. \tag{64}$$

Again, as in Section 3.1, the limit $\delta_C \ll \delta_T$ is equivalent to $Le \gg 1$.

(b) $\delta_C \gg \delta_T$

Omitting the details for brevity the results in this case are

$$\delta_C \sim HLe^{-1}(Ra^*)^{-1/(2n+1)} \tag{65}$$

$$Sh \sim Le(Ra^*)^{1/(2n+1)}. \tag{66}$$

3.2.2. *Mass transfer driven flow.* The velocity scale is obtained from equation (20) after neglecting the heat transfer contribution to the body force term and by invoking equation (56) to scale the concentration differences:

$$v \sim \left(\frac{mg\beta_C\rho_\infty \dfrac{w''\delta_C}{D}}{A}\right)^{1/n}. \tag{67}$$

The scale for the concentration boundary layer δ_C in equation (67) results from a scaling analysis of the

species concentration equation (5) in the region ($\delta_C xH$). The procedure is identical to that which led to equation (46) earlier. In the present case, the final result is

$$\delta_C \sim H\,Le^{-n/(2n+1)}(Ra^*)^{-1/(2n+1)}|G^*|^{-1/(2n+1)} \quad (68)$$

where the buoyancy ratio (for constant heat and species flux) is defined as

$$G^* = \frac{(\beta_C w''/D)}{(\beta q''/k)}. \quad (69)$$

Combining equations (62) and (68) yields the corresponding scale for the Sherwood number

$$Sh \sim Le^{n/(2n+1)}(Ra^*)^{1/(2n+1)}|G^*|^{1/(2n+1)}. \quad (70)$$

To obtain the scales of the characteristic heat transfer quantities in the mass transfer driven boundary layer flow, the energy equation is integrated in the x-direction between the wall and a point outside both boundary layers. The scaling equivalent of the resulting integral equation is identical to equation (50) with ΔT, given by equation (55), replacing the quantity $(T_o - T_\infty)$. As in earlier cases, two possibilities are considered to evaluate the quantity min (δ_T, δ_C).

(a) $\delta_T \ll \delta_C$

Here min $(\delta_T, \delta_C) = \delta_T$ and equation (50) yields

$$\delta_T \sim H\,Le^{1/2(2n+1)}(Ra^*)^{-1/(2n+1)}|G^*|^{-1/(2n+1)}. \quad (71)$$

Combining equations (60) and (71)

$$Nu \sim Le^{-1/[2(2n+1)]}(Ra^*)^{1/(2n+1)}|G^*|^{1/(2n+1)}. \quad (72)$$

As discussed before, the results (70) and (71) are valid if $Le \ll 1$.

(b) $\delta_T \gg \delta_C$

In this case, min $(\delta_T, \delta_C) = \delta_C$. Following identical procedure, it can be shown that in the present domain ($\delta_T \gg \delta_C$ or $Le \gg 1$)

$$\delta_T \sim H\,Le^{(n+1)/(2n+1)}(Ra^*)^{-1/(2n+1)}|G^*|^{-1/(2n+1)} \quad (73)$$

$$Nu \sim Le^{-(n+1)/(2n+1)}(Ra^*)^{1/(2n+1)}|G^*|^{1/(2n+1)}. \quad (74)$$

The main results for the scales of the various quantities in the case of constant wall heat and species fluxes are summarized in Table 2.

Before closing this section, it is worth discussing the range of validity of the scaling results (as well as the numerical results of the next section). Clearly, these results are valid when a double boundary layer structure (of the type shown in Fig. 1) is present in the system, a fact which is largely independent of the sign of the buoyancy ratio G or G^*. If the buoyancy ratio is negative as in the case of the mass transfer driven flow for example, the implication is simply that the fluid is traveling in the negative y-direction (opposite to what is depicted in Fig. 1). A question arises when the two contributions to the buoyancy force (temperature and concentration) are opposing each other, and, at the same time, they are of equal strength, i.e.

Table 2. Scales of various quantities of interest for a surface at constant heat and species flux

Driving potential		δ_T	δ_C	Nu	Sh
Temperature gradients, $\lvert G^*\rvert \ll 1$	$Le \gg 1$	$H(Ra^*)^{-1/(2n+1)}$	$H\,Le^{-1/2}(Ra^*)^{-1/(2n+1)}$	$(Ra^*)^{1/(2n+1)}$	$Le^{1/2}(Ra^*)^{1/(2n+1)}$
Temperature gradients, $\lvert G^*\rvert \ll 1$	$Le \ll 1$	$H(Ra^*)^{-1/(2n+1)}$	$H\,Le^{-1}(Ra^*)^{-1/(2n+1)}$	$(Ra^*)^{1/(2n+1)}$	$Le(Ra^*)^{1/(2n+1)}$
Concentration gradients, $\lvert G^*\rvert \gg 1$	$Le \ll 1$	$H\,Le^{1/2(2n+1)}(Ra^*\lvert G^*\rvert)^{-1/(2n+1)}$	$H\,Le^{-n/(2n+1)}(Ra^*\lvert G^*\rvert)^{-1/(2n+1)}$	$Le^{-1/2(2n+1)}(Ra^*\lvert G^*\rvert)^{1/(2n+1)}$	$Le^{n/(2n+1)}(Ra^*\lvert G^*\rvert)^{1/(2n+1)}$
Concentration gradients, $\lvert G^*\rvert \gg 1$	$Le \gg 1$	$H\,Le^{(n+1)/(2n+1)}(Ra^*\lvert G^*\rvert)^{-1/(2n+1)}$	$H\,Le^{-n/(2n+1)}(Ra^*\lvert G^*\rvert)^{-1/(2n+1)}$	$Le^{-(n+1)/(2n+1)}(Ra^*\lvert G^*\rvert)^{1/(2n+1)}$	$Le^{n/(2n+1)}(Ra^*\lvert G^*\rvert)^{1/(2n+1)}$

the buoyancy ratio is of the order of negative unity (G or $G^* \approx 0(-1)$). This situation was not encountered in the scaling analysis where only large (in the absolute sense) values of the buoyancy ratio were considered (G or $G^* \gg 1$, and G or $G^* \ll -1$). Clearly, when G or $G^* \approx 0(-1)$ the heat transfer driven flow will "collide" with the mass transfer driven flow which is of similar strength and travels in the opposite direction. In this case, the double boundary layer structure discussed earlier cannot exist and the present analysis does not apply. As will become obvious in the following section, numerical solutions of the boundary layer type in this regime fail to converge as well.

4. NUMERICAL SOLUTION

4.1. *Formulation of the similarity model*

The mathematical model for the general case of variable wall temperature consists of equations (1), (4), (5), (10), (11), (18), (19) and (20). This model accepts a similarity transformation in the limit of boundary layer approximations. The similarity variable is defined by observing the functional form of the scale for the thermal boundary layer thickness in the case of heat transfer driven flow with constant wall temperature and concentration [equation (25)]. This choice is based on the fact that it will yield a similarity variable which is independent of Le. To this end,

$$\eta = \frac{x}{y}(Ra_y)^{1/2n} \tag{75}$$

where

$$Ra_y = \frac{mg\beta\rho_\infty P y^{\lambda+n}}{A\alpha^n}. \tag{76}$$

Note that equation (26) becomes identical to equation (75) if H is replaced by y and equation (18) is used for T_0. Introducing the streamfunction in the usual manner

$$u = \frac{\partial\psi}{\partial y} \quad v = -\frac{\partial\psi}{\partial x} \tag{77, 78}$$

we postulate that

$$\psi = \alpha Ra_y^{1/2n} f(\eta). \tag{79}$$

Combining equations (77)–(79) yields

$$v = -\frac{\alpha}{y} Ra_y^{1/n} f' \tag{80}$$

$$u = \frac{\alpha}{y} Ra_y^{1/2n}\left(\frac{\lambda+n}{2n} f + \frac{\lambda-n}{2n}\eta f'\right). \tag{81}$$

Utilizing equations (75), (80) and (81) we cast the conservation equation for momentum, energy and species in the following form:

$$f' = -(\theta + GS)^{1/n} \tag{82}$$

$$\theta'' = \frac{\lambda+n}{2n} f\theta' - \lambda f'\theta \tag{83}$$

$$S'' = Le\left(\frac{\lambda+n}{2n} fS' - \lambda f' S\right) \tag{84}$$

where the dimensionless temperature and species conservation are defined as

$$\theta(\eta) = \frac{T - T_\infty}{T_0 - T_\infty} \quad S(\eta) = \frac{C - C_\infty}{C_0 - C_\infty}. \tag{85, 86}$$

The similarity form of the boundary conditions is

$$\eta = 0: \quad f = 0 \quad \theta = 1 \quad S = 1 \tag{87)–(89}$$

$$\eta \to \infty: \quad f' = 0 \quad \theta = 0 \quad S = 0. \tag{90)–(92}$$

At this point, the similarity formulation of the problem is complete. Before proceeding with the numerical solution, several issues that will facilitate the solution process and the presentation of the results need to be discussed.

First it is obvious that by setting $\lambda = 0$ in the general model one recovers the limit of constant wall temperature and concentration. What is, however, the value of λ that yields the constant heat and mass flux limit? This value is obtained by evaluating the expression for the heat or mass flux at the wall. Choosing the former,

$$q''_{x=0} = -k\left(\frac{\partial T}{\partial x}\right)_{x=0} = kP^{2n+1/2n}\left(\frac{mg\beta\rho_\infty}{A\alpha^n}\right)^{1/2n} \times y^{\left(\frac{\lambda-n}{2n}+\lambda\right)}[-\theta'(0)]. \tag{93}$$

From equation (93), we easily arrive at the important result that for the wall heat flux to be constant (independent of y)

$$\lambda = \frac{n}{2n+1}. \tag{94}$$

It can be shown identically that the same value of λ yields a constant mass transfer rate at the wall. Hence, *the value of λ for constant heat and mass transfer rate at the wall depends on the power law exponent of the fluid saturating the porous matrix and it is fixed once the fluid is specified.* In the limit of Newtonian fluids ($n = 1$) equation (94) yields the well-known value $\lambda = 1/3$ [20]. Substituting equation (94) into equations (82)–(84) one obtains the similarity conservation equations for the case of constant wall heat and mass fluxes (not shown here for brevity). It is worth noting however that one can arrive at these equations independently if the thickness of the thermal boundary layer for the case of heat transfer driven flow from a constant heat and species flux wall, equation (58), had been used in place of equation (25) to construct the similarity variable and, subsequently, the similarity model. Note that, with the general formulation of the mathematical model, the boundary conditions for the constant heat and mass flux remain identical to equations (87)–(92).

Another interesting finding is extracted utilizing the expression for the total amount of energy or species convected at any location y. Opting for the former,

$$E(y) = \rho_\infty c_p \int_0^\infty v(T-T_\infty)\,dy$$

$$= -\alpha\rho_\infty c_p \left(\frac{mg\beta\rho_\infty P}{A\alpha^n}\right)^{1/2n}$$

$$\times P y^{[\lambda(1+2n)+n]/2n} \int_0^\infty f'(\eta)\theta(\eta)\,d\eta. \quad (95)$$

Note that the value of the energy integral, equation (95), increases with y if

$$\lambda > -\frac{n}{1+2n} \quad (96)$$

(n is a positive number).

More importantly, the energy integral (95) is independent of y if

$$\lambda = -\frac{n}{1+2n}. \quad (97)$$

The same result is obtained if the species convection integral instead of the energy integral of equation (95) is evaluated. Hence, the value of λ given by equation (97) corresponds to the case of heat and mass transfer from a constant heat and mass flux horizontal line source embedded in a porous medium. In the limit of $n = 1$ equation (97) yields the earlier published value $\lambda = -1/3$ for this configuration [20].

The similarity model outlined above [equations (82)–(92)] was solved using the integral method [21, 22]. To initiate the numerical solution process, the temperature and concentration fields were guessed to vary linearly between $\eta = 0$ and $\eta = \eta_\infty$ while satisfying the boundary conditions given by equations (88) and (89) and equations (91) and (92), respectively. To satisfy the boundary conditions at infinity, an integration distance $\eta_\infty = 10$ was found to be adequate. The iterative integration procedure was repeated until the convergence was obtained in terms of the criterion

$$\max|F^i(\eta) - F^{i+1}(\eta)| \leqslant 10^{-5} \quad (98)$$

where F represents $f(\eta)$, $\theta(\eta)$ and $S(\eta)$. The iteration number is denoted by i. The integration was performed using the trapezoidal rule with a step size $\Delta\eta = 0.001$. To obtain the solution, for the negative values of the buoyancy ratio G (opposing flows), the similarity momentum equation (82) was modified as

$$f' = -(-\theta - GS)^{1/n} \quad (99)$$

because the flow occurs in the negative y-direction.

The local heat and mass flux at the wall was calculated in terms of the local Nusselt and Sherwood numbers that are defined as follows:

$$Nu = \frac{q''_{x=0}\,y}{(T_0 - T_\infty)k} = -\theta'(0)Ra_y^{1/2n} \quad (100)$$

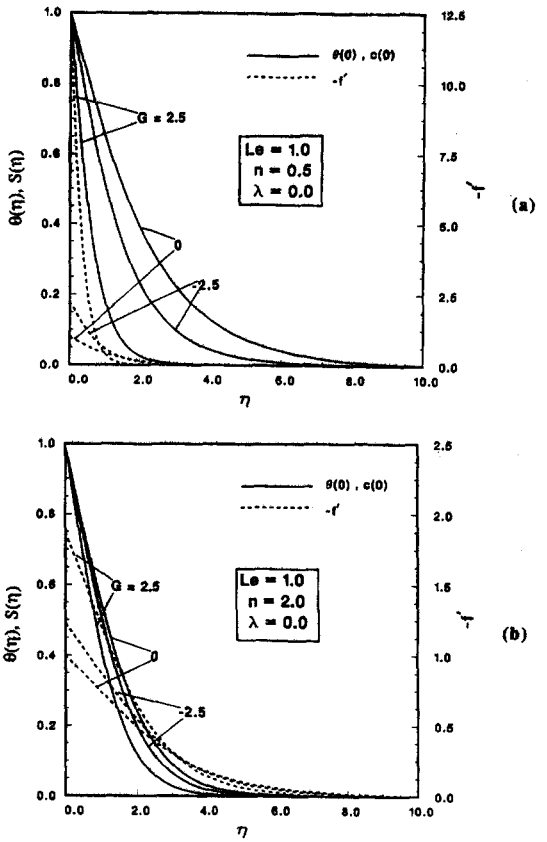

Fig. 2. The effect of buoyancy ratio on temperature, concentration, and velocity profiles for a surface with constant temperature and concentration: (a) $n = 0.5$; (b) $n = 2.0$.

$$Sh = \frac{w''_{x=0}\,y}{(C_0 - C_\infty)D} = -S'(0)Ra_y^{1/2n}. \quad (101)$$

4.2. *Discussion of numerical results*

The numerical solution of the mathematical model outlined in Section 4.1 aims at determining the effect of the main parameters of the problem on the temperature and concentration fields in the system and on the heat and mass transfer rates at the vertical surface. The accuracy of the numerical solution was tested by reproducing the results reported in ref. [3] in the limit of Newtonian fluid ($n = 1$) and constant temperature and concentration at the surface ($\lambda = 0$).

The discussion of the results starts with the effect of the buoyancy ratio on the temperature, concentration, and velocity distributions. To this end, Fig. 2 shows temperature, concentration, and velocity profiles in the double-diffusive boundary layer structure for a pseudoplastic fluid [$n = 0.5$, Fig. 2(a)], as well as for a dilatant fluid [$n = 2$, Fig. 2(b)] saturating the porous matrix, for a host of values of the buoyancy ratio, G. The wall temperature is modeled as isothermal and of constant concentration ($\lambda = 0$) and the Lewis number is set equal to unity rendering the thermal boundary layer identical to the concentration boundary layer in this illustrative case. The solid lines in Fig. 2(a) and

(b) represent the temperature and concentration distributions and the dashed lines the vertical velocity component distribution. In all cases, the temperature and concentration decrease monotonically away from the wall. For $G = 0$ (flow driven by temperature gradient alone) the thermal and velocity boundary layers are the thickest and the temperature, concentration, and velocity gradients at the wall the smallest. The value of $G = 2.5$ implies that the temperature and concentration buoyancy effects drive flows in the same direction (aiding one another). Indeed, this case yields the thinnest boundary layer and the sharpest gradients at the wall. When the thermal buoyancy opposes the concentration buoyancy in a flow moving in the direction of concentration buoyancy, $G = -2.5$, the flow, temperature, and concentration layers thicken as compared to the case of $G = 2.5$ and the corresponding gradients at the wall decrease. While Fig. 2(a) and (b) exhibits similar qualitative features, it is obvious that the effect of G becomes weaker as the value of the power law exponent increases from $n = 0.5$ in Fig. 2(a) to $n = 2$ in Fig. 2(b). Furthermore, the velocity boundary layer is thinner than the thermal and concentration boundary layers for pseudoplastic fluids ($n = 0.5$), whereas the velocity boundary layer is thicker than the thermal and concentration boundary layers for dilatant fluids ($n = 2$). Velocity, temperature, and concentration distributions, when constant heat and mass transfer rates are produced at the wall [$\lambda = n/(2n+1)$], also exhibited similar patterns. The corresponding figures are not shown here for brevity.

The effect of the Lewis number on the local Nusselt and Sherwood numbers, equations (100) and (101), is shown in Fig. 3(a)–(d) for several values of the buoyancy ratio. Figure 3(a) and (b) shows the effect for a wall at constant temperature and concentration, whereas Fig. 3(c) and (d) illustrates the same effect for a wall with constant heat and mass flux. In both these cases, as the Lewis number increases, the heat transfer rate at the wall decreases and the mass transfer rate increases. The effect of Le becomes weaker as the buoyancy ratio decreases. For $G = 0$ (flow driven by temperature gradient alone) the heat transfer rate is independent of Le. As the Lewis number approaches zero (species diffusivity much larger than thermal diffusivity), the heat transfer rate at the wall becomes practically independent of the Lewis number for all values of the buoyancy ratio. In the other extreme (as Le becomes very large), the heat transfer rates at the wall for various values of G approach asymptotically plateau values as well. Furthermore, the mass transfer rate is significantly increased as Le increases. The

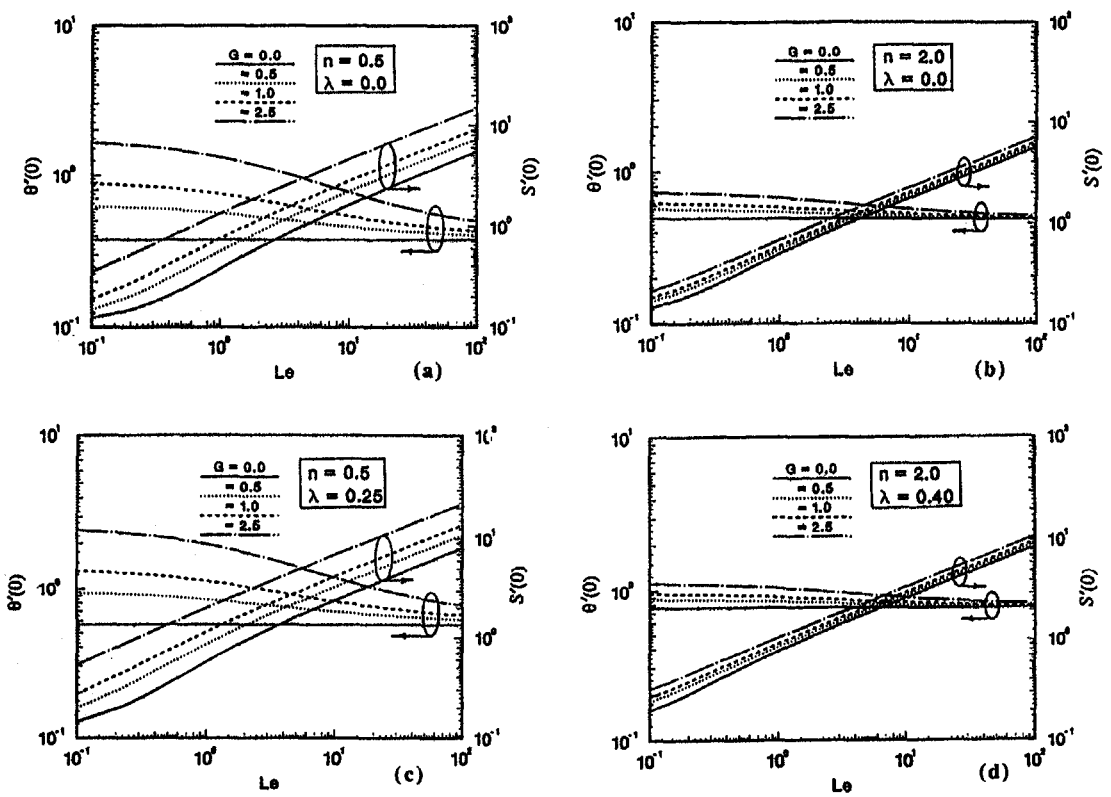

Fig. 3. The dependence of the local heat and species transfer rates on the Lewis number: (a) for a wall with constant temperature and concentration, $n = 0.5$; (b) for a wall with constant temperature and concentration, $n = 2.0$; (c) for a wall with constant heat and species flux, $n = 0.5$; and (d) for a wall with constant heat and species flux, $n = 2.0$.

effect of Le on the heat and mass transfer rates at the wall is more prominent for $n = 0.5$ compared to $n = 2$ for all values of the buoyancy ratio.

Figure 4 shows the variation of the quantity $-\theta'(0)|G|^{-1/2n}$ with the buoyancy ratio G for several values of the power law exponent. Note that the Lewis number is set equal to unity, and the wall is modeled as isothermal and of constant concentration. In the limit of $|G| \gg 1$ the scales given in Table 1 combined with equations (100) and (101) suggest that the order of magnitude of $-\theta'(0)|G|^{-1/2n}$ should approach a constant of order unity. Clearly, Fig. 4 illustrates this trend for the values of $|G| \gg 1$. Furthermore note that no similarity solution could be obtained for the values of the buoyancy ratio in the regime $-1 < G < 0$ and for $Le = 1$. As mentioned earlier in Section 3.1, when the buoyancy effects due to temperature and concentration gradients are of the same order of magnitude and in opposite directions, similarity formulation breaks down as the double boundary layer structure ceases to exist.

Next, we examine the effect of the power law exponent on the heat and mass transfer rates at the wall. To this end, Fig. 5(a) shows the results for an isothermal and constant concentration wall ($\lambda = 0$) whereas Fig. 5(b) contains the results for a wall with constant heat and mass flux [$\lambda = n/(2n+1)$]. The Lewis number is unity in both these figures. For aiding flows ($G = 0.5, 1$) the temperature and concentration gradients at the wall decrease with increasing values of n. For the flow driven by the temperature gradient alone ($G = 0$), the temperature and concentration gradients at the wall also decrease with an increase in the power law exponent. The opposite trend is found for opposing flows with $G = -2$. Interestingly, this trend will not be true for all opposing flows. For example, a close scrutiny of equations (82) and (99) reveals that for a Lewis number of unity a value of $G = -3$ will yield results identical to those of the aiding flows with $G = 1$ [note that the right hand side of equations (82) and (99) becomes identical for the two cases]. In the latter case, as discussed earlier, the temperature and concentration gradients decrease with increasing value of n. Note further that heat and species transfer rates at the wall become independent of the power law exponent in the range $n > 2$ for all values of the buoyancy ratio.

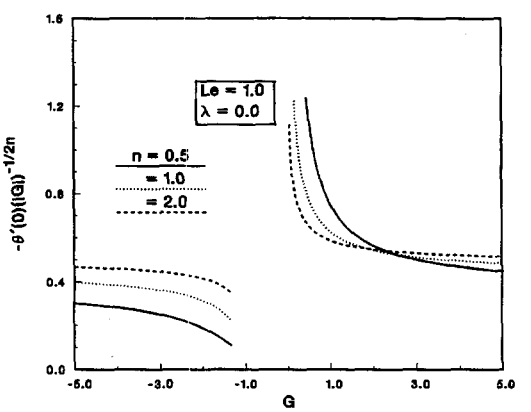

Fig. 4. The effect of buoyancy ratio on the quantity $\theta'(0)|G|^{-1/2n}$ for a wall with constant temperature and concentration.

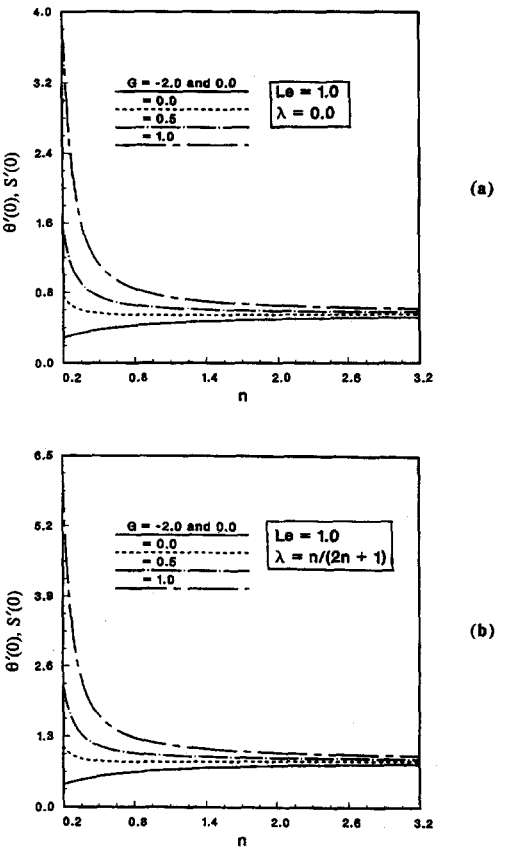

Fig. 5. The dependence of the local heat and species flux on the power law exponent: (a) for a surface at constant temperature and concentration and (b) for a surface at constant heat and species flux.

The effect of parameter λ on the temperature and concentration gradients at the wall is shown in Fig. 6 for three different values of n while the Lewis number is kept equal to unity. The parameter λ is varied between $-n/(2n+1)$ and unity. This figure presents two sets of curves, one corresponding to $G = -2$ (opposing flows) and the other to $G = 1$ (aiding flows). For both these stability ratios and for all fluids, an increase in value of parameter λ results in an increased value of the heat and mass transfer rates at the wall. Clearly, for $G = 1$, the effect of the parameter λ on the local heat and species flux is the greatest for $n = 0.5$ and the least for $n = 2$, while the opposite is true for $G = -2$.

5. CONCLUSION

This paper presented a fundamental study of the phenomenon of double-diffusion near a vertical sur-

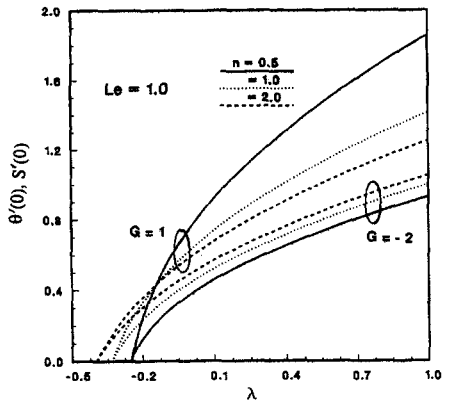

Fig. 6. The effect of the parameter λ on the local heat and species transfer rates.

face embedded in a fluid-saturated porous medium. The novel feature of the present study lies in the fact that the fluid saturating the porous matrix is non-Newtonian (power law). The first part of the study reported the scales of various quantities of interest such as the thickness of the thermal and concentration boundary layers as well as the Nusselt and Sherwood numbers for two limiting cases: (a) wall at constant temperature and concentration and (b) wall with constant heat and species flux. In the second half of the study, a mathematical model was pieced together and solved numerically so as to obtain the solutions for the above-mentioned two cases and to document the effect of various problem parameters on the velocity, temperature, and concentration fields, as well as the local heat and mass transfer rates.

The results indicate that the velocity boundary layer is thinner than the thermal and concentration boundary layers for dilatant fluids ($n > 1$). The opposite is true for pseudoplastic fluids ($n < 1$). An increase in the Lewis number results in a smaller local Nusselt number and a higher local Sherwood number at the vertical surface. For a fixed Lewis number, a higher value of the buoyancy ratio leads to enhanced temperature and concentration gradients at the wall compared to the same gradients for the flows driven by the temperature gradient alone. The effect of the Lewis number and the buoyancy ratio on the local heat and species flux at the wall is more prominent for fluids with $n < 1$.

For values of the power law index greater than two and for $Le = 1$, the local heat and species flux at the wall become independent of the power law index. An increase in the value of the parameter λ results in increased heat and species transfer rates at the wall for all fluids and all flows. It was found that the variation of the wall temperature and concentration necessary to yield a constant heat and species flux at the wall, depended on the power law index [equation (94)].

REFERENCES

1. D. Poulikakos, On buoyancy-induced heat and mass transfer from a concentrated source in an infinite porous medium, *Int. J. Heat Mass Transfer* **28,** 621–629 (1985).
2. S. E. Larson and D. Poulikakos, Double-diffusion from a horizontal line source in an infinite porous medium, *Int. J. Heat Mass Transfer* **29,** 492–495 (1986).
3. A. Bejan and K. R. Khair, Heat and mass transfer by natural convection in a porous medium, *Int. J. Heat and Mass Transfer* **28,** 909–918 (1985).
4. J. Y. Jang and W. J. Chang, The flow and vortex instability of horizontal natural convection in a porous medium resulting from combined heat and mass buoyancy effects, *Int. J. Heat Mass Transfer* **31,** 767–777 (1988).
5. J. Y. Jang and W. J. Chang, Transient free convection with mass transfer from an isothermal vertical flat plate embedded in a porous medium, *Int. Commun. Heat Mass Transfer* **15,** 17–30 (1988).
6. J. Y. Jang and J. R. Ni, Transient free convection with mass transfer from an isothermal vertical flat plate in a porous medium, *Int. J. Heat Fluid Flow* **10,** 59–65 (1989).
7. D. A. Nield, Onset of thermohaline convection in a porous medium, *Water Resour. Res.* **11,** 553–560 (1968).
8. W. J. Taunton and E. N. Lightfoot, Thermohaline instability and salt fingers in a porous medium, *Physics Fluids* **15,** 553–560 (1968).
9. B. Selimos and D. Poulikakos, On double diffusion in a Brinkman heat generating porous layer, *Int. Commun. Heat Mass Transfer* **12,** 149–158 (1985).
10. N. Rundraiah, P. K. Srimani and R. Friedrich, Finite amplitude convection in a two-component fluid saturated porous layer, *Int. J. Heat Mass Transfer* **25,** 715–722 (1982).
11. G. Z. Gershuni, E. M. Zhukhovitskii and D. V. Lyubimov, Stability of stationary convective flow of a mixture in a vertical porous layer, *Fluid Dynamics* **15,** 122–127 (1980).
12. A. A. Khan and Zebib, Double diffusive instability in a vertical layer of a porous medium, *J. Heat Transfer* **103,** 179–181 (1981).
13. H.-T. Chen and C.-K. Chen, Free convection flow of non-Newtonian fluids along a vertical plate embedded in a porous medium, *J. Heat Transfer* **110,** 257–260 (1988).
14. D. Poulikakos and T. L. Spatz, Non-Newtonian natural convection at a melting front in a permeable solid matrix, *Int. Commun. Heat Mass Transfer* **15,** 593–603 (1988).
15. H. Pascal, Rheological effects of non-Newtonian behavior of displacing fluids on stability of a moving interface in radial oil displacement mechanism in porous media, *Int. J. Engng Sci.* **21,** 199–210 (1983).
16. H. Pascal and J. P. Pascal, Non-linear effects of non-Newtonian fluids on natural convection in a porous medium, *Physica* D **40,** 393–402 (1989).
17. A. V. Shenoy, Non-Newtonian fluid heat transfer in porous media, *Adv. Heat Transfer* **24,** 101–190 (1994).
18. D. Getachew, Non-Newtonian convection in a porous matrix: constitutive equations and an application, Ph.D. Thesis, University of Illinois at Chicago (1994).
19. A. Bejan, *Convection Heat Transfer*. John Wiley, New York (1984).
20. P. Cheng and W. J. Minkowycz, Free convection about a vertical flat plate embedded in a porous medium with application to heat transfer from a dike, *J. Geophys. Res.* **82,** 2040–2044 (1977).
21. W. J. Minkowycz and E. M. Sparrow, Numerical solution scheme for local nonsimilarity boundary-layer analysis, *Numer. Heat Transfer* **1,** 69–85 (1978).
22. W. J. Minkowycz, E. M. Sparrow, G. E. Schneider and R. H. Pletcher, *Handbook of Numerical Heat Transfer*. John Wiley, New York (1988).